A 3D Virtual Radar System for Prediction and Evaluation of Radar Sensor Performance in Traffic Monitoring

Chengcheng Jiang[*], Yan Wu[+], Jean-Paul Linnartz[+], Marco Haverlag[+] and Xin Wang[+]
[*] Department of Mechanical Engineering, Hangzhou Dianzi University, China
[+]Eindhoven University of Technology, The Netherlands

***Abstract*—Radar sensors are widely used in intelligent transportation systems. The performance of radar sensors in practical setups depends on many factors, such as sensor specifications, choice of locations, height and orientations of sensor installation. Currently, most of these choices are made by a "rule of thumb". In many cases, trial and error changes of settings are required and several rounds of on-site measurements and adjustments are incurred, which are both inefficient and costly. To overcome these problems, this paper reports a 3D virtual radar system that can accurately predict and evaluate the performance of actual radar sensors using a standard computer. The proposed system builds upon a 3D virtual model of real world. It allows users to freely enter specifications for radar sensors and the underlying algorithm can efficient calculate and represent graphically in the 3D model by the coverage area of the chose radar sensors at the specified location in the virtual world. Comparison with experimental data obtained using hardware testbeds shows the result obtained by the virtual radar system is accurate.**

Keywords-Radar Sensor; Sensor; Sensors;Traffic Monitoring; Software performance modeling;

I. INTRODUCTION

Due to worldwide increase in population, urbanization and motorization, traffic intensity has grown significantly in the past few decades, especially in mega cities. This causes a fast increase in traffic congestion, which reduces transportation efficiency and increases air pollution. As a result, intelligent transportation systems are deployed worldwide to improve the management of traffic flow and road safety. Radar sensors are widely used in intelligent transportation systems for traffic monitoring applications including vehicle detection and tracking, speed measurements, due to their robustness in low light and bad weather conditions. The performance of radar sensors in practical varies based on the choices on sensors with different specifications, locations, height and orientations of sensor installation. Most of these choices are made as a "rule of thumb" and it is often unclear whether the chosen solution is the best in terms of performance, cost and safety.

Outdoor planning software built on 3D visualization tools are popular in many applications, such as navigation (Google Street view, Microsoft Street slide), Road/traffic planning and management (products of Cyclomedia, Yotta DCL), Environmental preservation (Carbon Calculator of CyberCity 3D) and radio frequency planning tools for GSM, UMTS *etc.* Building on this trend, in this paper, we propose a virtual radar system that can accurately predict and evaluate the performance of actual radar sensors. To develop such a virtual radar system, we aim at modeling existing city infrastructures like buildings, greeneries and city furniture to analyze and evaluate the mutual influence of such infrastructures on the deployment of new techniques for radar sensor systems. To realize this, we first need to construct a 3D virtual world with the city infrastructures. On top of this, we further implement "enhanced reality" to allow the dynamic inclusion of different sensors, sensor placements, virtual people, vehicles, street furniture etc. so as to study their influence on the radar sensor system. In this paper, we present a first look on the 3D virtual radar system we are developing. We use the 3D model "Campus2020" developed for the Eindhoven University of Technology (TU/e) campus in the department of architecture of TU/e as the baseline. To evaluate the accuracy of the performance obtained using the virtual radar system, we compared it with the experimental data obtained through measurement using a hardware testbed in the TU/e campus. The results from the virtual radar system show good agreement with the experimental data.

II. SYSTEM DESCRIPTION

There are many 3D generation and visualization tools developed in the market. Therefore, instead of developing a new 3D visualization tool, we used an existing tool and extended the functions based on this tool. Autodesk 3DS Max was selected as our 3D visualization tool because it is commonly accepted by users [1] for similar applications and allows easy development of new customized plug-ins. Fig. 1 shows a screenshot of the *De Zaale* street of the TU/e campus in the 3DS Max model. The reason we choose *De Zaale* street is that there are two hardware testbeds installed on the street

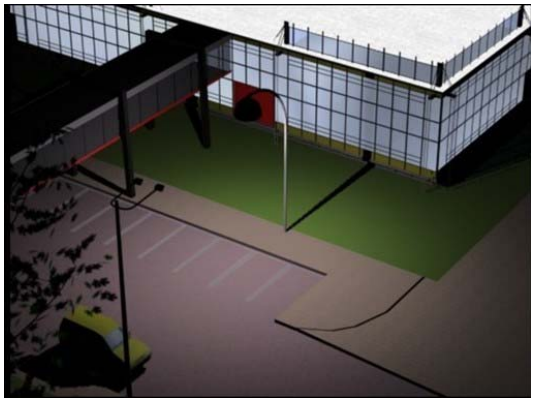

Figure 1. Screen shot of *De Zaale* street in the campus 2020 model.

978-1-4673-0990-5/12/$31.00 ©2012 IEEE

with radar and camera sensors, using which we can validate our results obtained using the virtual radar system.

The system also has a graphic user interface (GUI) using which the users can freely specify parameters for radar sensors. An illustration of the GUI is shown in Fig. 2. On the left, the user can enter antenna-related parameters such as antenna type, number of elements, element spacing, while on the right, the users can enter transceiver related parameters such as transmission power, noise figure (NF) and also the azimuth and elevation angles of the radar sensors. By clicking coverage areas, the underlying scripts will be invoked to calculate the coverage area for the specifications entered with algorithms that will be presented in Section III.

With the calculated coverage area for a specified detection probability and false alarm rate, the developed virtual radar system also plots this area graphically on the 3D virtual world to provide an intuitive illustration. An example of such an illustration is shown in Fig. 7.

III. PREDICTION OF THE RADAR SENSOR PERFORMANCE

The procedure for obtaining the coverage area for a given type of radar sensor is illustrated in Fig. 3. The radar performance is usually measured in terms of detection

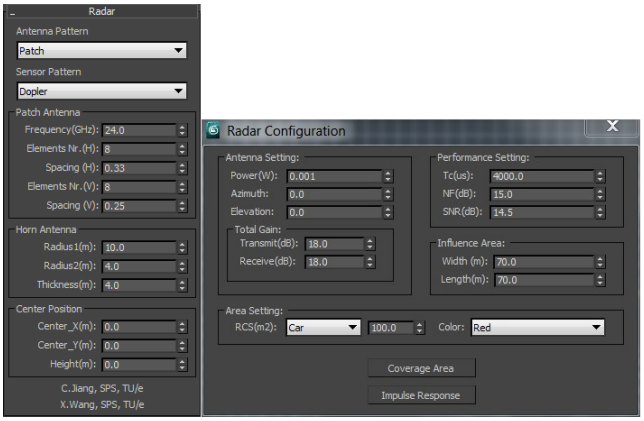

Figure 2. Graphical user interface (GUI) used for entering radar sensor specifications.

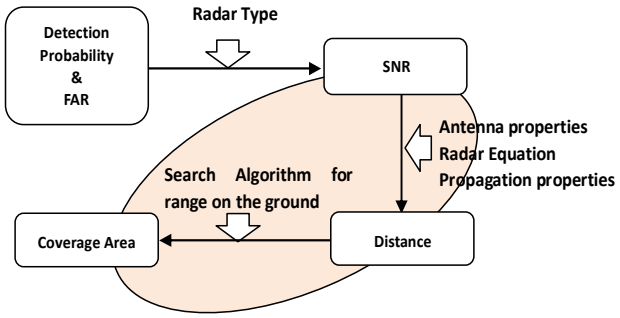

Figure 3. Procedures for obtaining coverage area from the radar specifications.

probability and false alarm rate (FAR). From the requirements on detection probability, FAR and the radar type, e.g. doppler or frequency modulated continuous wave (FMCW), entered by the user, a required signal to noise ratio (SNR) on the received signal can be calculated [2] [3]. Based on the user-specified radar sensor parameters, the underlying scripts calculate the detection range, i.e. the longest distance between radar and targets that radar can detect in a certain direction. With the obtained detection range, by using the search algorithm explained in section III.B, the virtual radar system will calculate the coverage area on the ground, which is relevant for traffic monitoring applications. The coverage area is defined as the area where the detection probability is above a predefined threshold. Based on this performance prediction function, users are allowed to import various kinds of virtual radar sensors to the 3D environment and to calculate the coverage area for the current radar setup.

A. Cacluation of detection range

The SNR at a radar receiver can be calculated as

$$\mathrm{SNR} = \frac{P_r}{P_n} = \frac{P_r}{B10^{(-174-30+\mathrm{NF})/10}} \tag{1}$$

The P_r here is the received signal power, and P_n is the average power of noise. Measurement bandwidth is represented by B. NF is noise figure of the radar receiver and the power spectrum density of thermal noise if -174dBm/Hz. The receive Power P_r can be calculated from the well-known radar equation [4]:

$$P_r = \frac{P_t G_t G_r \xi \lambda^2}{4\pi^3 d^4} \quad , \tag{2}$$

where P_t is the transmit signal power, G_t is the transmit antenna gain, G_r is the receive antenna gain and ξ is radar cross section (RCS) of the target. Symbol λ is used to represent the wavelength and d is the distance of the target. Using (1) and (2), we can derive the distance d as a function of SNR:

$$d = \sqrt[4]{\frac{P_t G_t G_r \xi \lambda^2}{4\pi^3 \mathrm{SNR} B 10^{(-174-30+\mathrm{NF})/10}}} \tag{3}$$

Parameters P_t, NF and B are set by the user. The unit for P_t is Watts and RCS (ξ) has the unit of m². For the RCS parameter, we allow users to select object type, such as "automobile", while a typical RCS value is provided according to [4], or users can enter the customized value for RCS.

We introduced a method to calculate the detection range for a specific SNR value. In the applications targeted in this paper, we are only interested in detecting vehicles on the ground. Therefore, we need to find detection distances which have intersection points with the ground or within 1 meter higher than the ground. As the first version, we only considered the main beam. The side lobe can be plotted using the same algorithm as the main lobe, but it was not implemented when we wrote this paper.

B. Search algorithm to obtain the coverage area

A simplified formulation of the coverage area is a description that, for every view angle from the radar sensor, gives the farthest and nearest range of reliable radar sensing. In fact this does not accommodate situations in which a hole in the coverage occurs between the main lobe looking towards the horizon and a side lobe covering the ground underneath the sensor pole. Our present implementation of algorithms determines one inner point (larger negative elevation angle) and one outer point at near-zero elevation.

In the inner part of the coverage area, the detection performance is limited by lower antenna gain outside the main direction.

The outer part consists of points of maximum range, where due to a smaller elevation angle the corresponding to antenna gain is near its maximum. In the outer part, the detection probability is limited by the (free space) path loss. We use two angles θ and φ to represent the orientation in the local coordinate system. The differences between θ, φ and the commonly used elevation and azimuth angles will be explained shortly. Vertical searching means to search the intersection points by φ, meanwhile horizontal searching is to process the vertical searching for each θ. For the horizontal searching, we change the value of θ with a step size Δθ. So for the *m*-th step, the angle for the horizontal searching θ_m is defined by:

$$\theta_m = m\Delta\theta,$$

$$m \in (0, m_{\max}) \text{ and } \Delta\theta = \pi/(m_{\max}+1)$$

For each value of θ, we define a vertical plane as the sample space for vertical searching, which consists of all end points of detection range on orientations with the same θ.

Fig. 4 shows a vertical plane with θ=π/2. The value of φ is from 0 to π. Considering only the main beam of the radar antenna, we can see it has two intersection points with the ground. As we explained before, point *a* is the outer point while point *b* is the inner point. There are two situations that the vertical plain crosses the ground, which are with one intersection point or with two intersection points. For the situation which the vertical plane has only one intersection point with the ground, we treat it as a special case, where the inner and outpoints coincide.

Fig. 5 is a simplified version of flow chart for the search algorithm in radar performance prediction function. It only shows the search algorithm for the main lobe, which covers the horizontal angle from θ_{n1} to θ_{n2}. Here we use θ_{n1} and θ_{n2} to denote the angles of two first nulls in the antenna beam pattern. The algorithm can be extended to cover the sidelobes in a similar manner. In each vertical plane inside the main lobe with $\theta = \theta_m$, we start the vertical searching from $\varphi = \pi/2$, that is where the peak gain occurs. After that, we do an iterative calculation as explained in Fig. 5. We calculate d_0 for φ_0 equal to π/2 degree first, the gain is G (θ_m,π/2). The variable φ_0 is in radar's local coordinate system, which is the angle with axis y_0 in Fig. 6. The rAngle in Fig. 6 is the elevation angle.

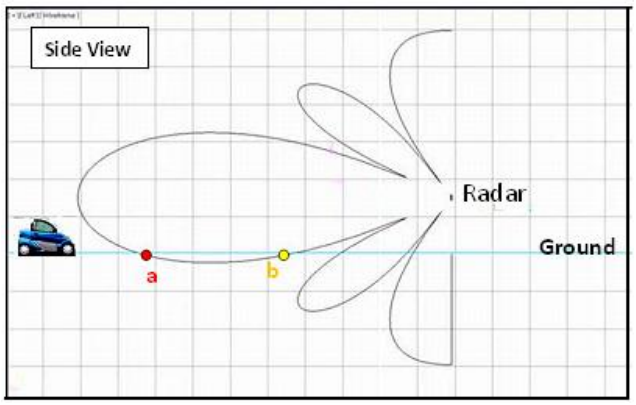

Figure 4. Side view of vertical plane for θ= π/2.

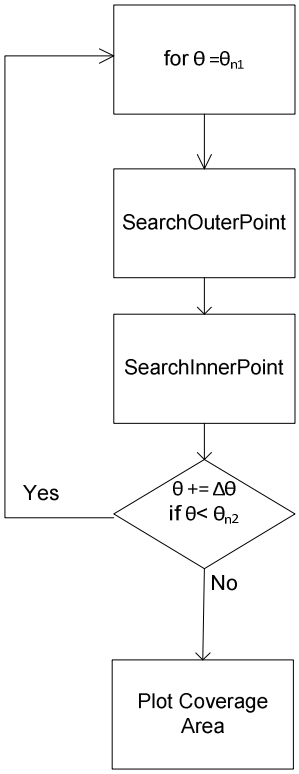

Figure 5. Flow chart of the search algorithm.

The elevation angle is the angle between the direction of the geometric center of the radar and the (idealized) horizon. It equals to -7° for the example shown in Fig. 6. We try to project it to the ground with the same distance d_0. The height of radar is represented by h_R, which is the Z value of the radar position in the world coordinate system. The Z value of the ground in the world coordinate is h_G. Then *h* is the distance between the radar and ground

$$h = h_R - h_G$$

So we get r_1 by

$$r_1 := \sqrt{d_0^{\,2} - h^2}$$

and the corresponding angle φ_1 is:

$$\varphi_1 := \tan^{-1}\left(\frac{r_1}{h}\right) - \text{rAngle}$$

But according to the radiation pattern of main beam, $G(\theta_0,\varphi_1) < G(\theta_0,\varphi_0)$, so at φ_1 the SNR at a range of r_1 is smaller than the targeted SNR. In fact, the detection distance is d_1 in direction φ_1. Then we do the above calculation again. The i-th iterative calculation is

$$r_i := \sqrt{d_{i-1}^{\,2} - h^2}$$

$$\varphi_i := \tan^{-1}\left(\frac{r_i}{h}\right) - \text{rAngle}$$

$$G_i := G(\theta_0, \varphi_i)$$

$$d_i := f(G_i)$$

The iteration stops when the radiation reaches the ground. We defined a maximum number of iteration times to avoid infinite iteration when the vertical plane has not across with the ground. We limit the number of iterations to a maximum of 5 because good visual accuracy occurred within 3 iterations already. We checked whether the ray reaches the ground by calculating the end point $P_e(x,y,z)$ of the radiation ray, and checked whether the Z values of this end point $P_e.z$ are in the range (h_G, $h_G + \Delta h$) in the world coordinate system. Δh is the height of object. We used 1 meter in this paper because our targets are predominantly cars. Once $P_e.z$ satisfies this criterion, we store the φ value as φ_{out} and the end point P_e as P_{eo}. This algorithm is quite fast, based on our result, 3 times iteration are on average enough for us to find the convergance point.

The inner convergance point occurs at an angle smaller than φ_{out}, but larger than the angle φ_{n1} of the first null. So we find that the searching angle φ_s must satisfy

$$\varphi_{n1} < \varphi_s < \varphi_{out}$$

To accelerate the searching procedure, we start the searching procedure from the intermediate value φ_2, which is

$$\varphi_2 = \varphi_{n1} + (\varphi_{out} - \varphi_{n1})/2$$

The algorithm checks whether $P_e.z$ is larger than h_G, which represent whether P_e is above the ground. If it is above the ground, the searching space will between φ_2 and φ_{out}, if not, the searching space will between φ_{n1} and φ_2. It is clearer to indicate it by code:

//**********/

if $P_e.z < h_G$ then

for $\varphi_s = \varphi_{n1}$ to φ_2 do

(searching inner point)

else if $P_e.z > (h_G+1)$ then

for $\varphi_s = \varphi_2$ to φ_{out} do

(searching inner point)

/**********//

Once we found the inner point, we store the φ_s value as φ_{inner} and the end point P_e as P_{ei}. An example is shown in Fig. 7. The effects of elevation angles on the coverage areas, which would require time- and labour-consuming adjustments and measurements in conventional systems, are clearly visible graphically.

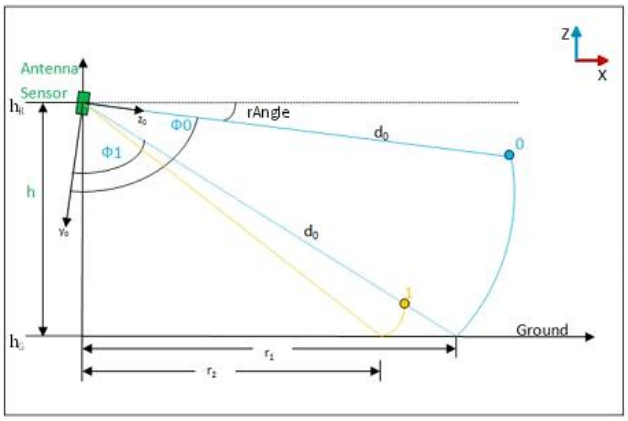

Figure 6. Side view of algorithm for outer points searching in plane $\theta = \theta_m$.

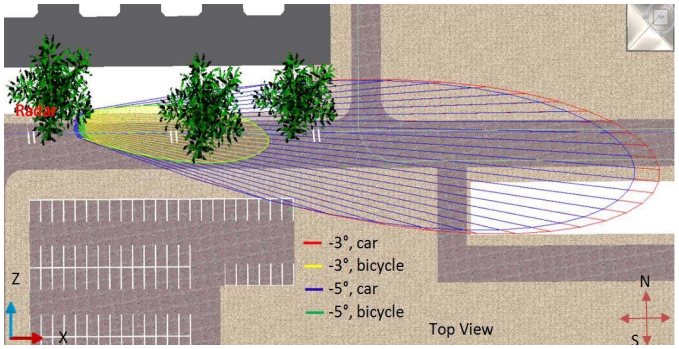

Figure 7. Coverage area for cars with different elevation angles(rAngle).

TABLE 1: Parameters settings for the testbed experiements

Parameters	**Value**
Height	4 (m)
Detection probability	95%
FAR (False Alarm Rate)	0.1%
Pt	0.001 (watts)
Peak Gain (transmit)	18 (dB)
Peak Gain (receive)	18 (dB)
NF	15 (dB)
Frequency	24 (GHz)
ξ (car)	100(m^2)
Antenna Spacing	0.6λ

IV. PERFORMANCE ANALYSIS

To evaluate the modeling accuracy of radar sensor, we compare it with the experiment data obtained using the hardware testbed in *De Zaale* street. The radar sensor in the testbed is mounted on a light pole at a height of 4 meters. Detection probabilities and FAR are statistical quantities and are difficult to measure in experiments. We thus compare the received radar signal power, which is directly related to SNR and the detection performance, calculated using the virtual radar system with that measured with the hardware testbed for three different experiments. The radar transceiver used in the testbed is the K-MC1 tranceiver by RFbeam Microwave GmbH [5]. Some key parameters used in the experiments are summarized in Table 1.

Fig. 8 shows the comparison of received power as a function of the distance between the targets (cars) and the light pole, where the radar sensor is mounted. To avoid discrepancies due to unknown amplifier settings in the hardware, we scaled the received signals for the three experiments by the same factor such that the maximum power of middle experiment is equal to 1. We normalize the received power by the virtual radar system in the same way. The comparison shows good agreements between the experimental data and data predicted by the virtual radar system for distances up to 100 m. For distances above 100 meters, the received power in the hardware systems reaches the error floor thus it does not go down any more as distance increases. The dip in received power at a distance of about 15 meters is due to the first antenna null between the main lobe and second lobe in the beampattern of the antenna array in the radar sensor. This is captured reasonably accurately by the virtual radar system.

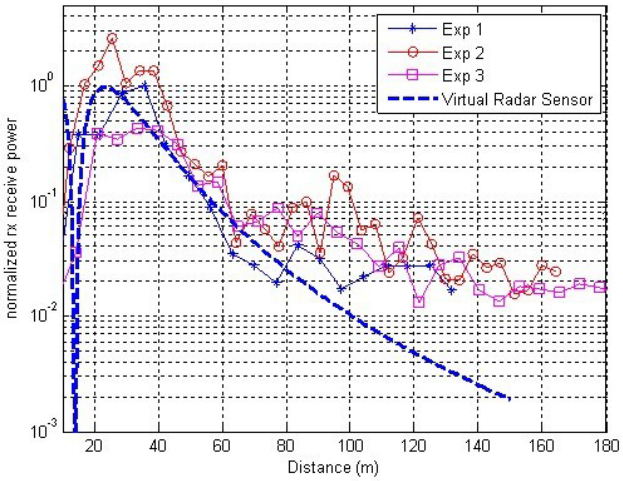

Figure 8. Comparison of received power obtained using the virtual radar sensor system and hardware experiments.

V. CONCLUSION

In the context of 3DS MAX, we have developed a system to predict and evaluate the performance of actual radar sensors for traffic monitoring. This system has allowed us to benefit from the efficient modeling and visible representation of radar performance. We have shown how to modeling the radar system by customized parameters. Moreover, the system can easily be extended for additional functions, which is part of our future work.

VI. ACKNOWLEGEMENT

This work was supported in part by the Netherlands Knowledge Worker project ENSURE.

REFERENCES

[1] W. Wang, "Research of traffic safety simulation based on 3ds max," in Proc. Int. Conf. Computer Modeling and Simulation ICCMS '09, 2009, pp. 307–309.

[2] A. G. Stove, "Linear FMCW radar techniques," IEE Proceedings F Radar and Signal Processing, vol. 139, no. 5,pp. 343–350, 1992.

[3] D. O. North, "An analysis of the factors which determine signal/noise discrimination in pulsed-carrier systems," Proc. IEEE, vol. 51, no. 7, pp.1016–1027, 1963.

[4] M.I. Skolnik, "Introduction to radar systems", 3rd Edition, Mc-Gram-Hill Ltd. , 2001.

[5] K-MC1 radar transceiver, http://www.rfbeam.ch/48.0.html.